Subpolar North Atlantic Mean State Affects the Response of the Atlantic Meridional Overturning Circulation to the North Atlantic Oscillation in CMIP6 Models

ANNIKA REINTGES,[a] JON I. ROBSON,[a] ROWAN SUTTON,[a] AND STEPHEN G. YEAGER[b]

[a] *National Centre for Atmospheric Science, University of Reading, Reading, United Kingdom*
[b] *National Center for Atmospheric Research, Boulder, Colorado*

(Manuscript received 8 August 2023, in final form 12 June 2024, accepted 1 July 2024)

ABSTRACT: The Atlantic meridional overturning circulation (AMOC) plays an important role in climate, transporting heat and salt to the subpolar North Atlantic. The AMOC's variability is sensitive to atmospheric forcing, especially the North Atlantic Oscillation (NAO). Because AMOC observations are short, climate models are a valuable tool to study the AMOC's variability. Yet, there are known issues with climate models, like uncertainties and systematic biases. To investigate this, preindustrial control experiments from models participating in the phase 6 of Coupled Model Intercomparison Project (CMIP6) are evaluated. There is a large, but correlated, spread in the models' subpolar gyre mean surface temperature and salinity. By splitting models into groups of either a warm–salty or cold–fresh subpolar gyre, it is shown that warm–salty models have a lower sea ice cover in the Labrador Sea and, hence, enable a larger heat loss during a positive NAO. Stratification in the Labrador Sea is also weaker in warm–salty models, such that the larger NAO-related heat loss can also affect greater depths. As a result, subsurface density anomalies are much stronger in the warm–salty models than in those that tend to be cold and fresh. As these anomalies propagate southward along the western boundary, they establish a zonal density gradient anomaly that promotes a stronger delayed AMOC response to the NAO in the warm–salty models. These findings demonstrate how model mean state errors are linked across variables and affect variability, emphasizing the need for improvement of the subpolar North Atlantic mean states in models.

KEYWORDS: Atlantic Ocean; Climate models; Model comparison; Model errors; Climate variability; North Atlantic Oscillation

1. Introduction

A unique climate component of the North Atlantic Ocean is the Atlantic meridional overturning circulation (AMOC). The AMOC is characterized by the northward flow of near-surface water high in temperature and salinity, balanced by a southward flow of cold water at middepth. These flows are linked by deep convection and water mass transformation in the subpolar North Atlantic, producing deep water (Lumpkin and Speer 2007; Buckley and Marshall 2016).

The AMOC is an important contributor to the total northward heat transport in the Northern Hemisphere (Trenberth et al. 2019; Rhines et al. 2008). Variability in the AMOC has been shown to affect weather and climate in Europe and North America (Rhines et al. 2008; Zhang et al. 2019; Sutton and Dong 2012). The AMOC exhibits considerable variability on decadal and multidecadal time scales (Danabasoglu 2008; Kwon and Frankignoul 2012; Zhang 2017; Wei and Zhang 2022). Thus, AMOC-related processes may be a source for predictability beyond subseasonal time scales (J. Robson et al. 2012; Yeager et al. 2012; Msadek et al. 2014; Zhang and Zhang 2015; Jackson et al. 2019) and make the North Atlantic stand out regarding its high potential for decadal predictability (Yeager and Robson 2017; Robson et al. 2018).

Given its key role in climate, there is a large interest in the future evolution of the AMOC. Model studies suggest that under greenhouse gas forcing, the AMOC will slow down (Weaver et al. 2012; Weijer et al. 2020). The expected slowing of the AMOC is associated with the projected increase of stratification in the high latitudes of the North Atlantic through surface freshening and warming. Yet, the strength of this expected decline is very uncertain (Reintges et al. 2017; Bellomo et al. 2021). It is under debate whether the AMOC has already decreased in the past (Caesar et al. 2018, 2021; Latif et al. 2022; Kilbourne et al. 2022) and whether this can be linked to anthropogenic forcing.

One important driver of AMOC variability is the North Atlantic Oscillation (NAO), as it generates both surface buoyancy and wind anomalies in the key regions affecting the AMOC. The NAO describes the sea level pressure difference between the Azores high and the Icelandic low. A positive (negative) NAO index refers to an anomalously high (low) pressure difference and stronger (weaker) westerlies, which are associated with temperature and precipitation anomalies across the North Atlantic sector and especially over Europe (Hurrell et al. 2003; Scaife et al. 2008, 2014), where the strongest impacts appear in boreal winter. Observation-based studies suggest that NAO forcing can modulate deep-water formation through altering surface buoyancy via freshwater,

Denotes content that is immediately available upon publication as open access.

Supplemental information related to this paper is available at the Journals Online website: https://doi.org/10.1175/JCLI-D-23-0470.s1.

Corresponding author: Annika Reintges, a.reintges@reading.ac.uk

DOI: 10.1175/JCLI-D-23-0470.1

heat, and momentum flux (Stramma et al. 2004; Yashayaev 2007). Various model studies provide evidence for the influence of the NAO on the AMOC (Delworth et al. 2017; Delworth and Zeng 2016; Lohmann et al. 2009; Megann et al. 2021; J. I. Robson et al. 2012; Schurer et al. 2023; Kim et al. 2020). The wind forcing of the NAO drives anomalies in the Ekman transport that are characterized by a convergence (divergence) at about 45°N for a positive (negative) NAO. This generates a dipolar response of the AMOC in z space which is positive (negative) in the south and negative (positive) in the north for the positive (negative) NAO (Khatri et al. 2022; Ortega et al. 2012). The wind-forced signal is thought to drive AMOC variability mostly on interannual and shorter time scales (Khatri et al. 2022; Kostov et al. 2021; Roach et al. 2022). In contrast, NAO-related turbulent heat fluxes (HFs) over the subpolar North Atlantic have been shown to drive (multi)decadal AMOC variability in model studies (Delworth and Zeng 2016; Yeager and Danabasoglu 2014; Megann et al. 2021; J. I. Robson et al. 2012; Schurer et al. 2023; Kim et al. 2024). The increased (reduced) buoyancy loss during a positive (negative) NAO affects the water mass transformation in the deep-water formation regions (Chafik et al. 2022; Ortega et al. 2017; Jackson and Petit 2023; Kim et al. 2021; Roussenov et al. 2022). This signal can be traced southward along the deep western boundary reaching subtropical latitudes after a few years (e.g., Polo et al. 2014).

As the AMOC is an integral metric referring to the basin-wide Atlantic zonal-mean volume transport, observations are challenging and, thus, limited in time and space. For the subtropics, there is the RAPID array (Cunningham et al. 2007) providing observational estimates for the AMOC at 26.5°N over the period 2004–22. The Overturning in the Subpolar North Atlantic Program (OSNAP) observing system (Lozier et al. 2017) is the basis for subpolar AMOC estimates and covers the period 2014–19. As these periods are too short for many research questions, climate models are a valuable tool widely used to study AMOC variability and, specifically, the NAO–AMOC interaction. However, because we rely on climate models, we have to be aware of their shortcomings, including model biases and uncertainties. Several variables in the North Atlantic are known to have large mean state biases in many models. This is the case for sea surface temperature (SST) and sea surface salinity (SSS) (Ba et al. 2014; Wang et al. 2014; Menary et al. 2015), Labrador Sea ice coverage and deep convection (Heuzé 2017), and mixed layer depths (Treguier et al. 2023). There is also a large spread across models regarding the mean state and variability of the AMOC (Xu et al. 2019; Cheng et al. 2013; Ba et al. 2014; Mecking et al. 2016, 2017; Wang et al. 2014; Jackson et al. 2020; Lai et al. 2022; Liu et al. 2022; Robson et al. 2022; Jackson and Petit 2023; Lin et al. 2023).

There are multimodel studies that investigated the effect of mean states on specific processes that might be relevant to the NAO–AMOC relationship. A phase 6 of Coupled Model Intercomparison Project (CMIP6) analysis by Jackson and Petit (2023) revealed that a high mean salinity in the Labrador Sea is linked to a higher mean and variability of the AMOC, in line with a prior study examining CMIP5 models (Mecking et al. 2017). Furthermore, Menary et al. (2015) found that in models with a warm and salty surface layer in the Labrador Sea, density variations are predominantly controlled by temperature variations, whereas in models with cold and fresh conditions, density variations are dominated by salinity variations. Because the AMOC is sensitive to deep-water formation in the Labrador Sea, model differences in the temperature and salinity of the subpolar gyre could be crucial for explaining differences in the NAO–AMOC link. Moreover, the Labrador Sea is a key region for NAO-related oceanic heat loss anomalies. The role of mean states in the subpolar North Atlantic is also emphasized in a recent study by Kim et al. (2023) who found that models with a strong NAO–AMOC relationship simulated less sea ice, deeper mixed layers, and stronger NAO-forced buoyancy fluxes. Lin et al. (2023) showed in a study on AMOC future projections that models with a strong mean AMOC had higher SSTs and SSS in the Labrador Sea. As this is also linked to a weaker stratification, the greenhouse gas–driven atmospheric forcing induced a larger oceanic heat gain which generated stronger subsurface density responses and a larger effect on the AMOC's decline. Large CMIP5 model disagreement in the NAO–AMOC relationship has also been demonstrated in a study by Xu et al. (2019). They found a larger spread across models in the coupled (ocean–atmosphere) compared to uncoupled (ocean-only with surface forcing) experiments, but the reason for that is still unknown.

Our main hypothesis is that surface mean state biases (warm–salty versus cold–fresh) in the North Atlantic subpolar gyre can explain a significant part of intermodel differences in the AMOC response to the NAO. We quantify the mean states' impacts on the NAO-forced AMOC response in time and space and then propose a mechanism explaining the physical links. Identifying key variables contributing to intermodel uncertainty is essential for meaningful interpretation of research findings based on models and, moreover, for future model improvement. In section 2, the climate models, observational datasets, and methods are described. Results are presented in section 3, demonstrating the differences across CMIP6 mean states and their effect on processes that influence the AMOC response to the NAO. A discussion is provided in section 4, and the summary and conclusions are provided in section 5.

2. Data and methods

a. Models

This study utilizes the output of CMIP6 of the World Climate Research Programme (WCRP). To investigate the internal variability across different climate models, the preindustrial control experiments (Eyring et al. 2016) are used here. This means that all variability is generated internally as there is no external forcing (e.g., from anthropogenic greenhouse gases or volcanic eruptions). Specifically, greenhouse gas concentrations are fixed to 1850 concentrations. A total of 47 coupled climate model variants are analyzed here (Table 1). They were selected based on data availability of the three-dimensional ocean temperature and salinity. As this study concerns the AMOC response to the NAO, the focus will be on a subsample of 27 models (listed in bold) that provide a long enough (minimum 100 years) overlapping period for the meridional overturning streamfunction and sea level pressure and are either listed in the

TABLE 1. Model variants analyzed from CMIP6. The first column refers to the model number used in Fig. 1. The last column indicates the category (cf. Fig. 1), where w/s means "warm–salty," c/f means "cold–fresh," "c/s" means "cold–salty," and "w/f" means "warm–fresh." Potential density and temperature, salinity, and mixed layer depth are available for all models. The availability of NAO, SIC, HF, and AMOC data is listed in separate columns. The third last column refers to the overlapping period of the NAO and AMOC data. From Fig. 2 and onward, only models listed in bold will be considered.

No.	Institute	Model	Variant	NAO	SIC	HF	AMOC	Length (yr)	Horizontal ocean resolution (°)	Category
1	AWI	AWI-CM-1-1-MR	r1i1p1f1	x		x			0.25 × 0.25	w/s
2	AWI	AWI-ESM-1-1-LR	r1i1p1f1	x		x			0.5 × 0.5	w/s
3	BCC	BCC-CSM2-MR	r1i1p1f1	x	x				1 × 1	w/s
4	BCC	BCC-ESM1	r1i1p1f1	x	x				1 × 1	w/s
5	CAMS	CAMS-CSM1-0	r1i1p1f1	x	x	x			1 × 1	c/f
6	CAS	FGOALS-f3-L	r1i1p1f1	x					1 × 1	c/f
7	**CAS**	**FGOALS-g3**	**r1i1p1f1**	**x**	**x**		**x**	**500**	**1 × 1**	**w/s**
8	**CCCma**	**CanESM5**	**r1i1p1**	**x**	**x**	**x**	**x**	**999**	**1 × 1**	**c/f**
9	**CCCma**	**CanESM5**	**r1i2f1**	**x**		**x**	**x**	**450**	**1 × 1**	**c/f**
10	CCCR-IITM	IITM-ESM	r11p1f1	x					1 × 1	c/s
11	CMCC	CMCC-CM2-SR5	r1i1p1f1	x	x	x	x	499	1 × 1	c/s
12	CNRM-CERFACS	CNRM-CM6-1	r1i1p1f2	x		x	x	499	1 × 1	c/s
13	**CNRM-CERFACS**	**CNRM-ESM2-1**	**r1i1p1f2**	**x**	**x**	**x**	**x**	**499**	**1 × 1**	**c/f**
14	CSIRO	ACCESS-ESM1-5	r1i1p1f1	x	x	x	x	999	1 × 1	w/f
15	**CSIRO-ARCCSS**	**ACCESS-CM2**	**r1i1p1f1**	**x**	**x**	**x**	**x**	**499**	**1 × 1**	**c/f**
16	**E3SM-Project**	**E3SM-1-0**	**r1i1p1f1**	**x**	**x**	**x**	**x**	**499**	**0.5 × 0.5**	**c/f**
17	**E3SM-Project**	**E3SM-1-1**	**r1i1p1f1**	**x**	**x**		**x**	**164**	**0.5 × 0.5**	**c/f**
18	**E3SM-Project**	**E3SM-1-1-ECA**	**r1i1p1f1**	**x**	**x**		**x**	**164**	**0.5 × 0.5**	**c/f**
19	**EC-Earth-Consortium**	**EC-Earth3**	**r1i1p1f1**	**x**	**x**	**x**	**x**	**356**	**1 × 1**	**c/f**
20	**EC-Earth-Consortium**	**EC-Earth3-LR**	**r1i1p1f1**	**x**	**x**	**x**	**x**	**183**	**0.5 × 0.5**	**c/f**
21	**EC-Earth-Consortium**	**EC-Earth3-Veg-LR**	**r1i1p1f1**	**x**	**x**	**x**	**x**	**499**	**0.5 × 0.5**	**c/f**
22	INM	INM-CM4-8	r1i1p1f1	x	x		x	530	1 × 1	c/s
23	**IPSL**	**IPSL-CM6A-LR**	**r1i1p1f1**	**x**	**x**	**x**	**x**	**1999**	**1 × 1**	**c/f**
24	**IPSL**	**IPSL-CM6A-LR**	**r1i2p1f1**	**x**	**x**	**x**	**x**	**249**	**1 × 1**	**c/f**
25	MOHC	HadGEM3-GC31-LL	r1i1p1f1	x	x	x	x	499	1 × 1	c/s
26	**MOHC**	**HadGEM3-GC31-MM**	**r1i1p1f1**	**x**	**x**	**x**	**x**	**499**	**0.25 × 0.25**	**w/s**
27	**MOHC**	**UKESM1-0-LL**	**r1i1p1f2**	**x**	**x**	**x**	**x**	**1879**	**1 × 1**	**c/f**
28	**MOHC**	**UKESM1-1-LL**	**r1i1p1f2**	**x**		**x**	**x**	**405**	**1 × 1**	**c/f**
29	**MPI-M**	**MPI-ESM1-2-HR**	**r1i1p1f1**	**x**	**x**	**x**	**x**	**499**	**0.4 × 0.4**	**w/s**
30	**MPI-M**	**MPI-ESM1-2-LR**	**r1i1p1f1**	**x**	**x**	**x**	**x**	**999**	**1.5 × 1.5**	**w/s**
31	NASA-GISS	GISS-E2-1-G	r1i1p1f1	x		x			1 × 1	w/s
32	**NASA-GISS**	**GISS-E2-1-G**	**r1i1p1f2**	**x**		**x**	**x**	**350**	1 × 1	**w/s**
33	NASA-GISS	GISS-E2-1-G	r1i1p1f3				x		1 × 1	w/s
34	NASA-GISS	GISS-E2-1-G	r2i1p1f1				x		1 × 1	w/s
35	NASA-GISS	GISS-E2-2-G	r1i1p1f1	x			x	150	1 × 1	c/s
36	**NCAR**	**CESM2**	**r1i1p1f1**	**x**	**x**	**x**	**x**	**1199**	**1 × 1**	**w/s**
37	**NCAR**	**CESM2-FV2**	**r1i1p1f1**	**x**	**x**	**x**	**x**	**499**	**1 × 1**	**w/s**
38	**NCAR**	**CESM2-WACCM**	**r1i1p1f1**	**x**	**x**	**x**	**x**	**498**	**1 × 1**	**w/s**
39	**NCAR**	**CESM2-WACCM-FV2**	**r1i1p1f1**	**x**	**x**		**x**	**499**	**1 × 1**	**w/s**
40	**NCC**	**NorCPM1**	**r1i1p1f1**	**x**	**x**	**x**	**x**	**498**	**1 × 1**	**w/s**
41	NCC	NorCPM1	r2i1p1f1						1 × 1	w/s
42	NCC	NorCPM1	r3i1p1f1						1 × 1	w/s
43	**NOAA-GFDL**	**GFDL-CM4**	**r1i1p1f1**	**x**	**x**	**x**	**x**	**499**	**0.25 × 0.25**	**w/s**
44	**NOAA-GFDL**	**GFDL-ESM4**	**r1i1p1f1**	**x**	**x**	**x**	**x**	**499**	**0.5 × 0.5**	**w/s**
45	NUIST	NESM3	r1i1p1f1		x				1 × 1	
46	**THU**	**CIESM**	**r1i1p1f1**	**x**			**x**	**499**	**0.5 × 0.5**	**w/s**
47	UA	MCM-UA-1-0	r1i1p1f1	x					2 × 2	c/s

warm–salty ("w/s") or cold–fresh ("c/f") category (see details in section 3a and Fig. 1).

b. *Observational data*

For comparison, we also incorporate observation-based reanalysis datasets; these include EN4 (Good et al. 2013) for temperature, salinity, and the calculation of density and mixed layer depth; HadSLP2 (Allan and Ansell 2006) for sea level pressure and the calculation of the NAO index; merged Hadley–NOAA/Optimal Interpolation (Hadley-OI) SST and sea ice concentration (SIC) (Shea et al. 2022) for SIC; and ERA5 (Hersbach et al. 2020) for the net surface heat flux. Note that

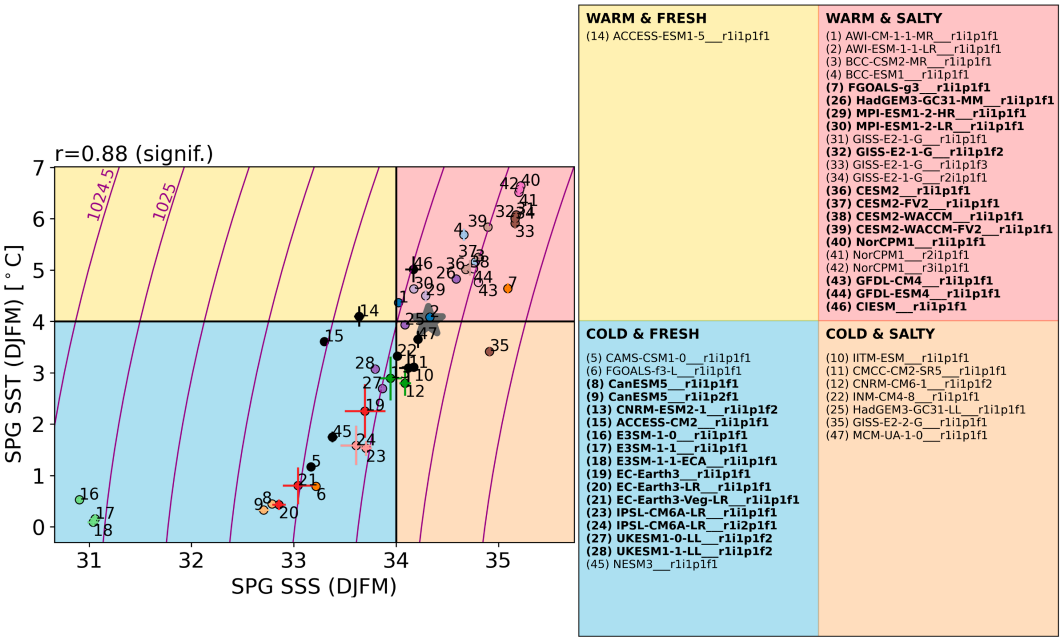

FIG. 1. Scatterplot of CMIP6 SPG surface mean states and their category: winter (DJFM) mean SPG (50°–65°N/65°–25°W) SSS vs SST. The background shading represents the category determined by the chosen category thresholds (34 psu for salinity and 4°C for temperature). Model variants are listed within their resulting category in the right panel (bold: model variants used for the subsequent analysis, cf. Table 1). Density contours (kg m^{-3}) are shown in purple. The crosses on top of the individual model dots indicate the standard error of the model means as a measure of uncertainty of the mean. Each dot represents an individual model, but we use colors other than black to highlight models from the same modeling center. The 1960–2022 EN4 mean is indicated by the gray star.

because observational uncertainty is larger in the earlier historical period, we only consider observations from 1960 onward. It must be noted that the real world has been subject to external forcing, whereas preindustrial experiments have not. Furthermore, observational ocean data from subsurface layers may still be subject to significant uncertainties after 1960. Given these two caveats, a comparison to reanalysis should be viewed with caution.

c. *Methods*

Data are used in annual resolution after averaging monthly model output. Data were averaged over boreal winter [December–March (DJFM)] when the effect of the NAO is expected to be largest. The AMOC is averaged over 12 months (August–July), resulting in the same centering as the DJFM-averaged variables. All data are linearly detrended. Where necessary, data were regridded to allow comparison across models. The NAO index is computed as the difference of winter (DJFM) sea level pressure between two small boxes, near the Azores (28°–20°W, 36°–40°N) and near Iceland (25°–16°W, 63°–70°N) as in Smith et al. (2020). Ocean potential density has been computed based on temperature and salinity. Additionally, individual contributions of potential temperature (salinity) to a change in potential density are computed, by allowing only potential temperature (salinity) to vary and keeping salinity (potential temperature) climatologically fixed. Ocean mixed layer depth is derived from the vertical change of potential density (DJFM averages), as the depth where potential density is 0.01 kg m^{-3} larger than at the surface.

For the AMOC, meridional overturning streamfunction CMIP6 output is used. As it is provided as a mass transport, it is converted into a volume transport assuming a constant density of 1000 kg m^{-3}. The resulting volume transport is presented in units of Sverdrup (Sv), where 1 Sv $\equiv 10^6$ m^3 s^{-1}. We note that the AMOC analysis here is based on the streamfunction in depth coordinates, which has been shown to have some difficulties in representing the high-latitude AMOC strength (Hirschi et al. 2020). However, due to the scarcity of CMIP6 data available for the overturning streamfunction in density coordinates, we opt to conduct the analysis with the overturning computed in depth coordinates.

All regressions presented here are linear regressions on the NAO index and are normalized by the standard deviation of the NAO index (σ NAO). To explore the significance of linear regressions, a bootstrapping technique has been applied: regressions were repeated with 1000 randomly generated NAO time series, sharing the same lag 1 year autocorrelation as the original NAO time series. Then, the original regression is tested against critical thresholds, the 2.5% or 97.5% percentile of these sample regressions, constituting a 95% confidence interval. If a number of model regressions are averaged, these averaged values are tested against the multimodel average of their critical threshold values. The significance of the difference between two model-averaged values (here: either climatological means or mean regressions) is tested through Welch's t test with a 95% confidence interval. For all tests, the effective number of degrees of freedom is applied, i.e.,

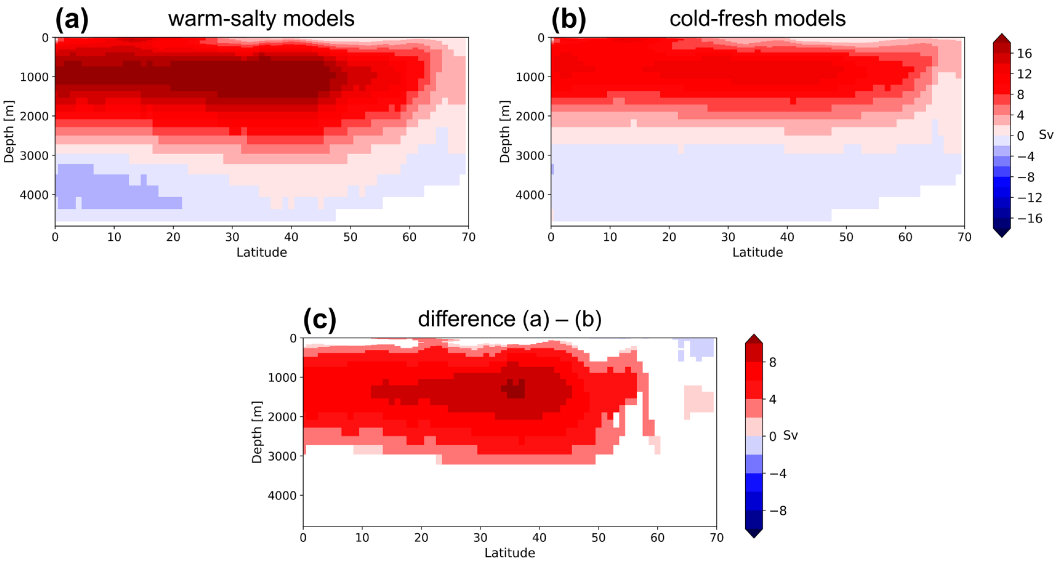

FIG. 2. Annual mean meridional overturning streamfunction averaged over (a) the warm–salty models, (b) the cold–fresh models, and (c) their difference where only significant differences are shown (see methods).

the decorrelation time scale is taken into account—estimated by the *e*-folding time scale of the autocorrelation (Leith 1973).

3. Results

a. Mean state and power spectrum differences

Within the 47 model variants analyzed here, there are large differences in the subpolar gyre mean states across CMIP6 models. Figure 1 shows that the winter (DJFM) SSS ranges from about 31 psu [Energy Exascale Earth System Model (E3SM)] to about 35 psu (NorCMP1) and the mean SST ranges from about 0°C (E3SM) to about 6.5°C (NorCPM1). Mean SSS and SST states for the models also correlate significantly ($r = 0.88$) based on a t test with a two-sided 95% confidence interval. For comparison, the EN4 mean of 1960–2022 is close to the multimodel mean of the SST and SSS model distribution. Although external forcing is present only in EN4, but not in these preindustrial model simulations, the effect of external forcing is relatively small (cf. Figs. 12a,b from Robson et al. 2022) compared to the spread across models which is approximately 4 psu in SSS and 7°C in SST. This spread in model states is similar to the CMIP5-based results of Menary et al. (2015) who found a somewhat lower spread of about 2.5 psu for salinity and the same spread of 7° for temperature despite averaging over the top 500 m of only Labrador Sea mean states.

Figure 1 also shows that warm–salty models are denser than the cold–fresh models, meaning that salinity is dominating mean surface density differences across the models. Nonetheless, an individual model's density variability could be salinity or temperature dominated. Menary et al. (2015) have shown that over the Labrador Sea, density variations in time in warm–salty (cold–fresh) models are temperature (salinity) dominated. Such differences in density drivers might have consequences for the response of the AMOC to the NAO and will be discussed below. To simplify the analysis, the models are categorized into either a warm–salty ("spicy") or cold–fresh ("minty") category. This categorization is based on thresholds of 34 psu for SSS and 4°C for SST that have been chosen that are close to the median of the distribution. The following analysis will focus on the differences between the warm–salty and cold–fresh categories, whereas models categorized as warm–fresh and cold–salty will be ignored. Furthermore, only models where data for the NAO and AMOC are available will be included in subsequent analyses. This results in 13 models in the warm–salty and 14 models in the cold–fresh category for the following analysis (respective models listed in bold in Table 1/right panel of Fig. 1).

Models that are warm–salty have a stronger and deeper upper meridional overturning streamfunction [North Atlantic Deep Water (NADW)] cell than cold–fresh models (Fig. 2). At about 35°N, the difference reaches ~10 Sv. This could be explained by a stronger AMOC causing a larger heat and salt transport into the subpolar gyre (SPG) region. Alternatively, a stronger AMOC in the warm–salty models could also be the result of the higher SSS causing a higher surface density and, hence, more deep-water formation in the high latitudes.

Significant differences are also apparent in the variability spectra of the North Atlantic between the two model categories. At 40°N, the AMOC variability on interannual and longer time scales is significantly stronger in the warm–salty models compared to the cold–fresh models (Fig. S2b in the online supplemental material). This is not seen, however, in the spectrum of the NAO index (Fig. S2c) and SST averaged over the subpolar North Atlantic (Fig. S2d). The NAO spectra of both model categories are relatively similar. The SST variability on all time scales is weaker in the warm–salty models compared to the cold–fresh models. Such reduced SST variability might be related to shallower mixed layers in the cold–fresh models (see below, Fig. 6). In those models, variability from atmospheric forcing might be limited to a relatively shallow layer, allowing larger amplitudes of variability at the surface.

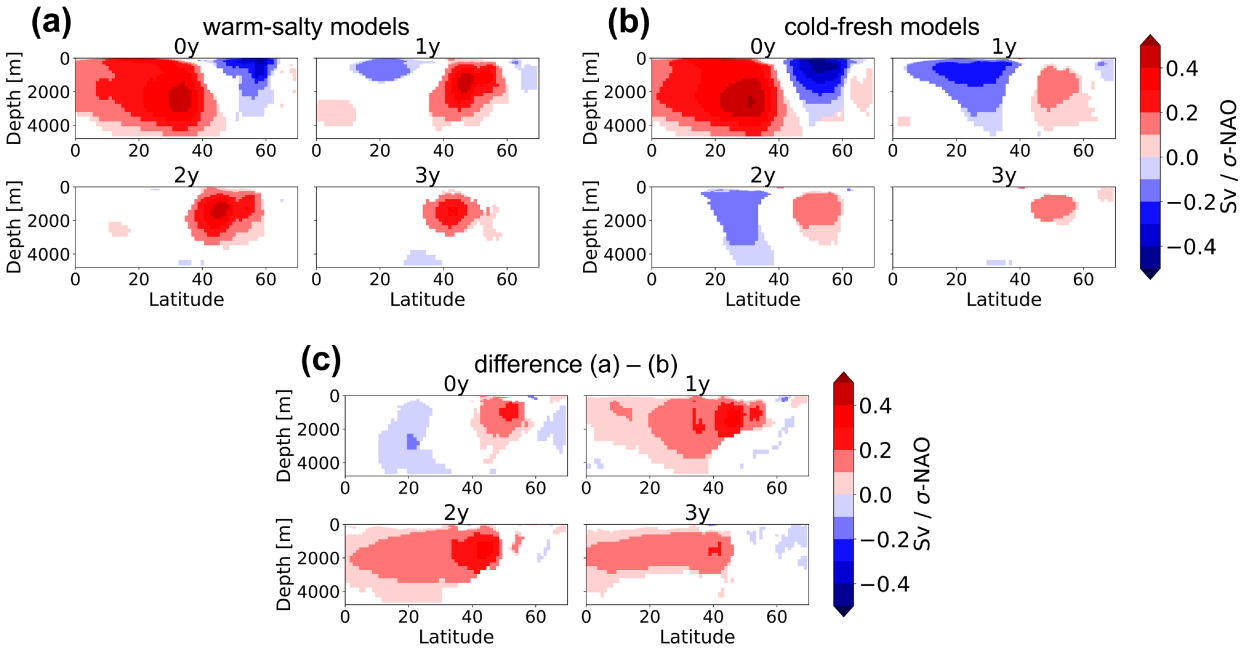

FIG. 3. Lagged latitude–depth AMOC regressions on the NAO index averaged over (a) the warm–salty models and (b) the cold–fresh models where only regressions are shown that are significant (methods). (c) Significant differences between the two model categories (see methods). The indicated lags portray the response 0–3 years after the NAO peak.

b. Differences in NAO–AMOC relationship

In this section, we demonstrate that the lagged AMOC response to the NAO differs between warm–salty and cold–fresh models. Figure 3 shows that there is an instantaneous dipolar response of AMOC to NAO at lag 0 years in both categories. This is largely a wind-driven response to the anomalous wind forcing of the NAO causing a northward Ekman transport anomaly south of about 45°N and a southward anomaly north of 45°N (cf. Fig. 4). However, the initial decrease of the subpolar AMOC is stronger in the cold–fresh models (Fig. 3c). This area is characterized by a subsequent strengthening from lag 1 year (i.e., when the NAO leads the AMOC by 1 year). This subpolar strengthening is stronger in the warm–salty models, and it persists over the following 2 years while also moving southward. Southward propagating signals in the AMOC forced by NAO-related heat fluxes have been found in previous model studies (Delworth and Zeng 2016; Delworth et al. 2017; J. I. Robson et al. 2012; Yeager and Danabasoglu 2014). This southward propagating signal is also revealed in the difference between the two categories (Fig. 3c), which is characterized by a latitudinally consistent pattern for the positive lags. In the cold–fresh models, this latitudinally coherent (and likely buoyancy related) signal could simply be too weak, compared to the dominating negative signal appearing in the subtropics (Fig. 3b). This negative response is consistent with a delayed wind-driven effect related to a Rossby wave adjustment in the density field, which will be discussed further in the subsection on the ocean density fingerprints.

The model category differences are also significant in the 5-year lowpass-filtered version of Fig. 3 (Fig. S5), suggesting that these differences stem from components of the NAO–AMOC interaction that last longer than just from year to year. At lag 2 and 3 years, the explained variance in the smoothed data of the warm–salty category reaches more than 16% (Fig. S6). The explained variances for the cold–fresh models in this latitude range are significantly lower.

The significant differences in the delayed AMOC response to the NAO are not caused by the wind-driven northward Ekman transport (computed from the zonally integrated Atlantic zonal wind stress), which is shown by Fig. 4. Consistent with Fig. 3, there are significant differences in the NAO–AMOC response at 26° and 40°N between the warm–salty (red) and cold–fresh (blue) models for the lags of 1–3 years (Figs. 4a–c). However, the correlation of NAO with the northward Ekman transport at these latitudes is not significantly different (see Figs. 4d–f). Furthermore, the NAO-related Ekman transport responds only instantaneously, and Ekman anomalies are negligible apart from lag 0 years. Therefore, it is likely that model differences in the AMOC–NAO link are related to the buoyancy forcing of the NAO.

We propose that the differences between the two model categories, as seen in their surface mean state and AMOC response to the NAO, originate from differences in the ocean and sea ice characteristics, rather than from differences in the NAO sea level pressure pattern itself or the NAO-related northward Ekman transport. This hypothesis is supported by (i) the overlapping power spectrum of the NAO index between model categories (Fig. S2c), (ii) the similarity of the northward Ekman transport response to NAO (Fig. 4), and (iii) the similar NAO sea level pressure pattern (Fig. S10). In particular, significant differences in the NAO sea level pressure over the North Atlantic Ocean are only found locally in the Labrador Sea.

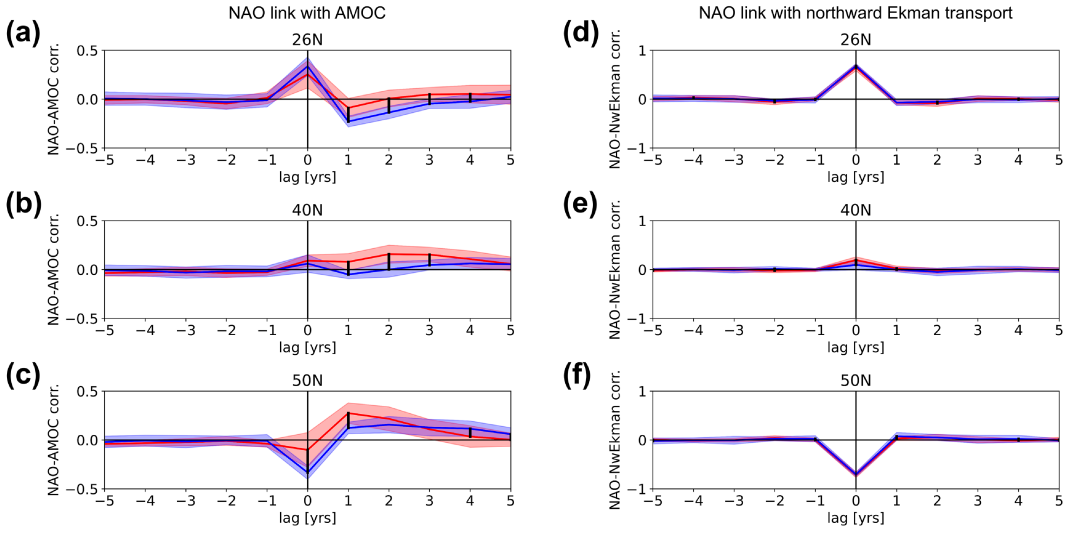

FIG. 4. Lagged correlations between the NAO index and the AMOC at (a) 26°N, (b) 40°N, and (c) 50°N and between the NAO index and the northward Ekman transport at (d) 26°N, (e) 40°N, and (f) 50°N. Red (blue) color represents warm–salty (cold–fresh) category, where the line is the category median and the shading is the interquartile range within the category. Significant differences between the means of the two model categories (see methods) are indicated by the thick vertical lines.

c. *Role of surface ocean characteristics in explaining intermodel differences in the NAO–AMOC relationship*

Consistent with the higher SPG–SSTs in the warm–salty models, there is a much lower winter (DJFM) mean sea ice concentration, particularly in the Labrador Sea (Fig. 5). Large parts of the Labrador Sea are ice-free in the warm–salty models. In contrast, the Labrador Sea in the cold–fresh models is largely ice-covered, and the ice edge is significantly further south. Over the Labrador Sea, the difference in sea ice concentrations between warm–salty and cold–fresh models reaches more than 60% (see Fig. 5c). In the east of the subpolar North Atlantic, both model categories have a similar sea

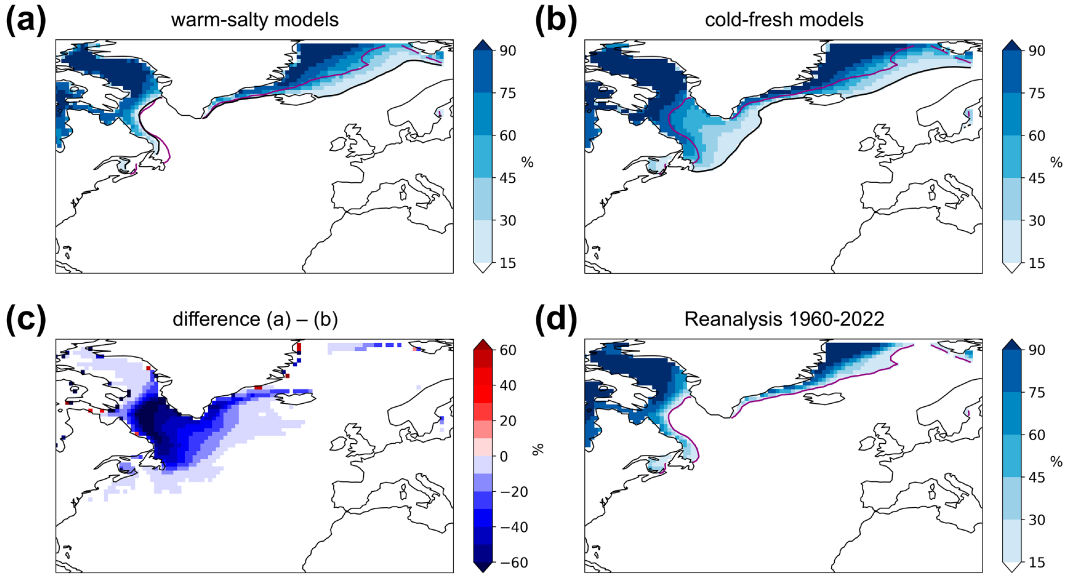

FIG. 5. Winter (DJFM) mean SIC (shading) averaged over (a) the warm–salty models, (b) the cold–fresh models, (c) their difference where only significant differences are shown (see methods), and based on (d) the reanalysis (merged Hadley-OI SST and SIC over 1960–2022). The sea ice edge (15% concentration threshold) for the respective model category averages is shown as the black lines in (a) and (b); the sea ice edge based on reanalysis is shown as the purple line in (a), (b), and (d).

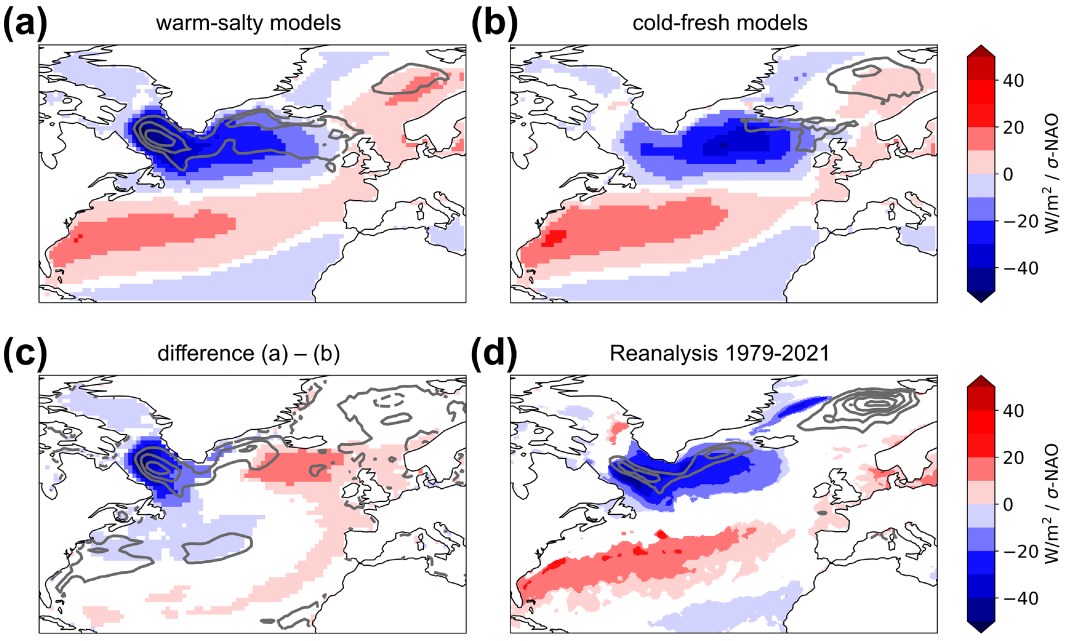

FIG. 6. Winter (DJFM) mean net surface downward HF regression on the NAO (shading) averaged over (a) the warm–salty models, (b) the cold–fresh models, (c) their difference where only significant differences are shown (see methods), and based on (d) the reanalysis (ERA5 HF and HadSLP2 sea level pressure over 1979–2021). In (a), (b), and (d), only regressions are shown that are significant (see methods). The contours in (a), (b), and (d) (based on EN4 over 1960–2022) indicate the winter (DJFM) mixed layer depth (300-m contour intervals), and those in (c) indicate the mixed layer depth difference between (a) and (b) (300-m contour intervals with differences equal or larger than zero in solid and negative difference in dashed).

ice concentration, except over parts of the East Greenland Current where warm–salty models have less ice cover. The low sea ice concentration in the warm–salty models is very similar to reanalysis data averaged over 1960–2022 (see Fig. 5d).

The oceanic heat loss over the Labrador Sea due to the NAO is also significantly smaller in the cold–fresh models compared to the warm–salty models (Fig. 6), consistent with the insulating impact of sea ice to air–sea heat exchanges. The regression of winter (DJFM) mean net surface downward heat flux on the NAO index reveals the well-known tripolar pattern (Visbeck et al. 2003) in both model categories (Figs. 6a,b) and in the reanalysis dataset (Fig. 6d). Yet, notable differences exist between the two model categories (Fig. 6c). In particular, the NAO-related oceanic heat loss is concentrated on the Labrador Sea in warm–salty models, whereas in the cold–fresh models, it is shifted to the east, to the southeast of the Irminger Sea. We speculate that turbulent fluxes, especially sensible heat fluxes, contribute most to the net surface flux differences, given that the differences in sea ice cover between the two model groups would also produce substantial differences in the air–sea temperature contrasts at the surface.

One variable that is linked to the heat flux pattern is the ocean mixed layer depth. Winter (DJFM) mean mixed layer depth is represented by the contours in Fig. 6. Deep mixed layers in the Labrador Sea of more than 800 m are found in the warm–salty models as well as in the EN4 data. However, such deep mixed layers are not present in the Labrador Sea in the cold–fresh models, but mixed layers in the Greenland–Iceland–Norwegian (GIN) Seas are deeper than warm–salty models. In EN4 data, the GIN Seas are characterized by very deep mixed layers of more than 1000-m depth. Such deep mixed layers may, however, also be the result of observational data errors—given the potential for large uncertainty in subsurface observations.

Labrador Sea mean stratification is also much weaker in the warm–salty models compared to the cold–fresh models based on profiles of potential density (Figs. 7a,b). This difference in stratification is due to the differences in the mean salinity profile (Fig. 7d) rather than the temperature profile (Fig. 7c). In particular, the cold–fresh models are characterized by an extremely low surface salinity, which yields a very stable water column in the upper few hundred meters of the Labrador Sea. The difference in stratification, therefore, implies that density stratification can be overcome more easily due to NAO-related surface heat flux forcing in the warm–salty models compared to the cold–fresh models.

Although the objective of this study is not to evaluate the realism of the model categories compared to observation, we find evidence that the warm–salty models provide are more realistic than the cold–fresh models (Figs. 6 and 7). Given the extremely high sea ice concentration in the cold–fresh models, we also suspect the sea ice mean state is more realistic in the warm–salty models despite the potential effects of external forcing (cf. Fig. 5).

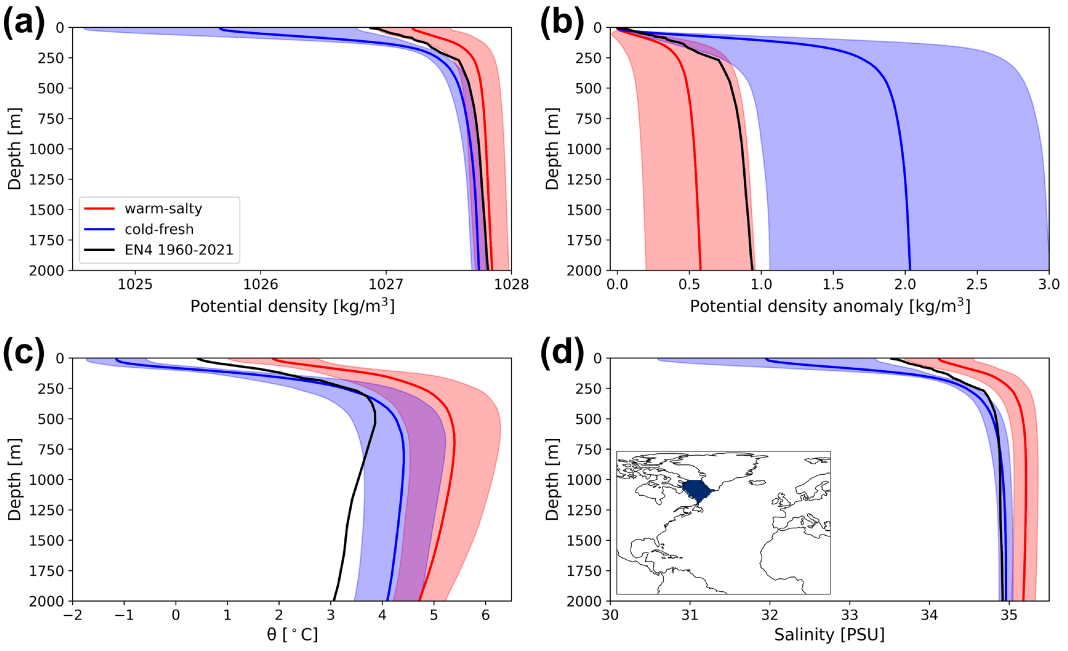

FIG. 7. Winter (DJFM) mean profiles averaged over the Labrador Sea area as shown in the subpanel of (d): (a) potential density, (b) potential density relative to the surface, (c) potential temperature, and (d) salinity. Red (blue) color represents warm–salty (cold–fresh) category, where the line is the category mean and the shading is the range of the standard deviation within the category. The black line is based on EN4 data averaged over 1960–2021.

d. *Exploring the ocean density fingerprints to explain the intermodel differences in the NAO–AMOC relationship*

The previous section showed that in warm–salty models, the Labrador Sea is not only the area with the largest NAO-related heat loss but also an area with relatively weak stratification. These differences have important implications for the NAO's potential to alter the AMOC through the generation of subsurface density anomalies because the NAO-related heat loss can potentially reach deeper ocean levels in the warm–salty models. This will be demonstrated in the following figures illustrating the lagged potential density regressions on the NAO at different depths.

Potential density changes at intermediate depths of 600-m depth (Fig. 8) reveal a stronger NAO-driven subsurface densification in the Labrador and Irminger Seas for the warm–salty models (Fig. 8a) compared to the cold–fresh models (Fig. 8b). Temperature regressions (Fig. S12) support that these differences in the temperature-driven density response are indeed associated with stronger subsurface cooling in the warm–salty models (rather than just being an effect of a different mean state). This densification persists until lag 3 years while it spreads somewhat southward (Fig. 8a). In the warm–salty models, the explained variance of this signal reaches 18%, 10%, and 5% in the subpolar gyre area, for lag 1, 2, and 3 years, respectively (Fig. S13). South of that densification signal, there is a reduction in density related to warming at about 35°–40°N, which is present in both model categories. This anomalous warming appears in the central North Atlantic at lag 0 years and subsequently propagates westward, consistent with the density signal found in Polo et al. (2014), and could explain the sign change of the subtropical AMOC response to the NAO seen in both model categories at lag 1 year (Figs. 3 and 4a). Polo et al. (2014) described this westward propagation as a Rossby wave signal excited by wind forcing on interannual time scales. The location of this light density anomaly at lag 0 years corresponds to an anomalous Ekman transport convergence that would be associated with the positive Azores sea level pressure anomaly (Figs. S10a,b). That the warm–salty models have a stronger subsurface response to the NAO in the subpolar North Atlantic is also apparent from the panel showing the model category differences (Fig. 8c). However, it is interesting that there is no significant difference in the subtropical density signal implying that the wind-forced density anomalies are broadly consistent between warm–salty and cold–fresh models.

At even greater depths of 1800 m (Fig. 9), there is also evidence that subpolar density anomalies are larger in warm–salty compared to cold–fresh models. In fact, there are hardly any significant anomalies in the cold–fresh model category (Fig. 9b). The panel showing the differences (Fig. 9c) therefore reflects the panel of the warm–salty models (Fig. 9a). In the warm–salty models, the temperature-related subsurface densification in the Labrador Sea (Fig. 9a and Fig. S14) starts to show 1 year after the NAO forcing, and it propagates southward along the western boundary over the following 2 years. The explained variance associated with this densification is largest for the lag of 3 years reaching 8% at the western boundary (Fig. S15). This signal is consistent with previous fingerprints of the buoyancy-forced AMOC adjustment (e.g.,

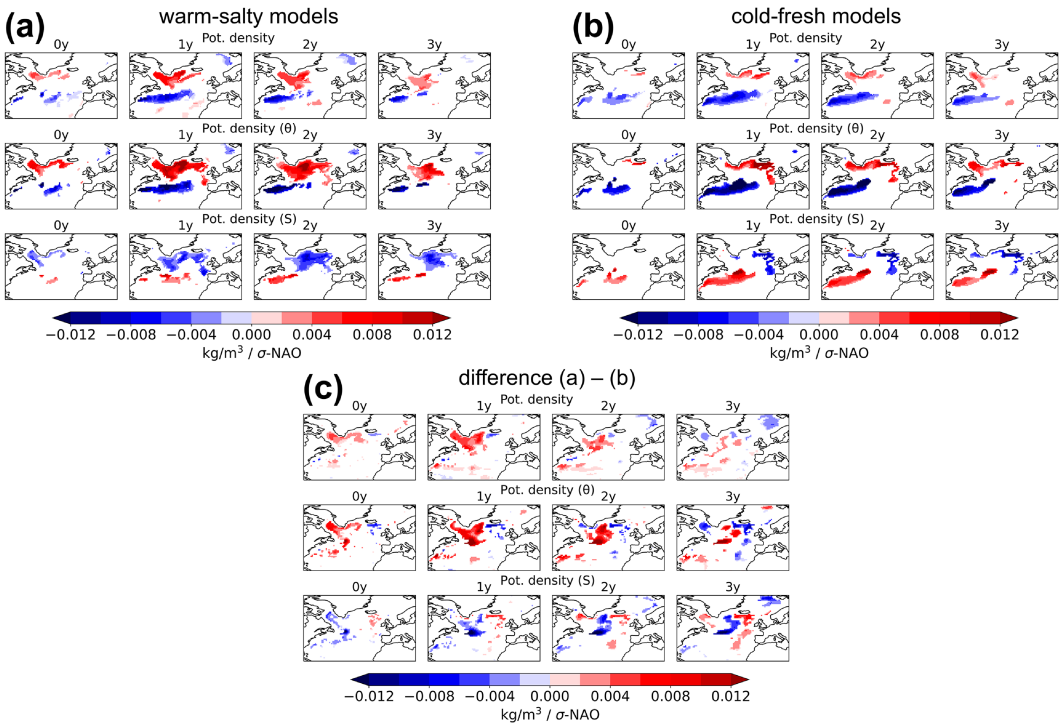

FIG. 8. Lagged regressions of winter (DJFM) potential density at 600-m depth on the NAO index averaged over (a) the warm–salty models and (b) the cold–fresh models where only significant regressions are shown (see methods). (c) Significant differences (see methods) between the two model categories. The indicated lags portray the response 0–3 years after the NAO peak. In addition to the full-density regressions, the contributions from temperature and salinity to density are shown separately.

Polo et al. 2014). A similar southward density propagation at a similar depth of 1795 m originating in the Labrador Sea is present in reanalysis followed by an AMOC increase (Jackson et al. 2016). The significantly larger density anomalies at depth in the warm–salty models are consistent with the differences in stratification and the differences in heat fluxes associated with NAO, which together allow a stronger connection of surface fluxes with the deeper ocean.

Because this deep density response is limited to the western boundary of the ocean basin, an anomaly in the zonal subsurface density gradient is created. Therefore, the delayed AMOC response to the NAO is consistent with the propagation of density anomalies on the western boundary and their impact on the circulation via the thermal wind balance. Such a delayed AMOC response to NAO forcing has been described in various studies (e.g., Khatri et al. 2022; Delworth and Zeng 2016; Megann et al. 2021; Polo et al. 2014).

4. Discussion

We have analyzed differences between models categorized based on their mean spiciness in the SPG of the North Atlantic (cf. summarizing schematic Fig. 10). Compared to the cold–fresh models, the Labrador Sea in the warm–salty models is characterized by a lower sea ice concentration, weaker stratification, and enhanced NAO-driven heat loss. This enables a deeper penetration of the NAO-related density signal, which then propagates southward along the western boundary. At 1800-m depth, this NAO density imprint is only present in the warm–salty models, where it creates a zonal density gradient anomaly which can explain the stronger delayed AMOC response in the warm–salty model category.

This study was motivated by the multimodel comparison study by Menary et al. (2015). They found that density variations over the Labrador Sea were temperature dominated in warm–salty models and salinity dominated in cold–fresh models. Their analysis focused on the top 500 m of the Labrador Sea. Comparing temperature and salinity contributions to the surface density regression in Fig. S16 reveals that the contribution of salinity in the lag 1–3 years is much more pronounced in the cold–fresh models, which is in line with the findings of Menary et al. (2015). Our findings also agree with the study by Kim et al. (2023). They demonstrate that in models with a stronger NAO–AMOC relationship, the Labrador Sea is characterized by a lower sea ice concentration and a weaker stratification and also that there is more NAO-related heat loss in those models. Furthermore, they find that the intermodel spread in the NAO–AMOC relationship is insensitive to the models' NAO amplitude. Our proposed mechanism is also in line with Lin et al. (2023). Although they focus on long-term trends of the AMOC under greenhouse gas forcing rather than on the impact of the NAO, they find that in models with a stronger mean AMOC, the Labrador Sea (LS) surface is warmer and saltier and that stratification is weaker, leading to

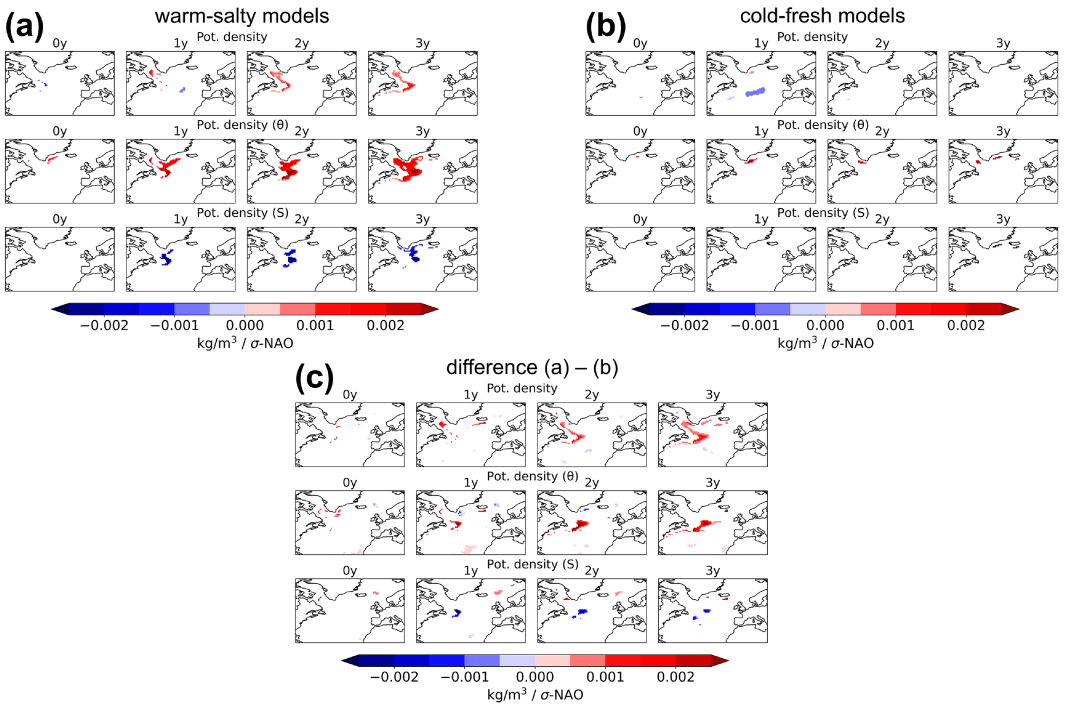

FIG. 9. As in Fig. 8, but for potential density at 1800-m depth.

larger subsurface density response to the warming signal, which then propagates southward along the western boundary and where it finally feeds back on the AMOC.

The density anomalies at depths below 500 m or even 1000 m seem to be essential for a strong, buoyancy-forced, meridionally coherent NAO–AMOC connection. This finding is in agreement with previous studies (Ortega et al. 2021; Polo et al. 2014; Yeager et al. 2021). The subsurface density signal (Figs. 8 and 9) appears with some delay to the NAO forcing and the surface response. The delayed response might be an effect of different processes, e.g., through a wind-driven compensating effect at lag 0 years, through additional anomalies originating in the Irminger Sea advected along the Greenland Current, through changes in mode water production propagating down in density space, and through exchanges between the interior and the boundaries. Another explanation might be that deep density signals could maximize in spring or summer, just a few months after the NAO forcing. Because of the DJFM averaging used here, such a signal could appear with a lag of 1 year.

Although the Labrador Sea stratification is weaker in the warm–salty category allowing the stronger delayed AMOC response, the GIN Seas stratification is weaker in the cold–fresh models (mixed layer depth contours in Fig. 6). Based on winter mixed layer depth and standard deviation, North Atlantic deep convection seems to be more pronounced in the Labrador Sea for warm–salty models and more in the GIN Seas for the cold–fresh models. This relationship is consistent with the CMIP6 analysis of Jackson and Petit (2023), who find the role of Labrador Sea processes to be smaller in models with a fresh Labrador Sea. Considering the entire North Atlantic, the cold–fresh models are on average characterized by a stronger stratification (contours in Fig. 6c). This could prevent NAO surface signals from reaching the deeper ocean (e.g., via deep water formation). As a result, NAO-forced variability is, compared to the warm–salty models, larger at the surface but smaller at deeper layers. This could explain that cold–fresh models compared to warm–salty models show higher variability in North Atlantic SST, while their AMOC (multi)decadal variability is lower (Fig. S2).

a. Sensitivity tests

The initial hypothesis that the AMOC response to NAO is sensitive to the models' mean SPG spiciness (i.e., the tendency to be warm and salty vs cold and fresh) has been confirmed. However, it is clear that some other metrics produce a large overlap in the model grouping compared to the original spiciness metric, given that physical links between the metrics exist. As a sensitivity test, we computed the lagged correlations between the AMOC at 40°N and the NAO index for a variety of metrics (Fig. S3), with the categorization used in this study shown in Fig. S3a. Based on the category differences and their statistical significance, surface spiciness (i.e., distinguishing between warm–salty and cold–fresh models) is one of the most important metrics to explain model differences. Nevertheless, there are other important mean state metrics. For example, it was shown that warm–salty models have a stronger mean AMOC (Fig. 2) and have their deepest mixed layers in the western subpolar North Atlantic (contours in Fig. 6). As a result, these metrics (Figs. S3g,i) produce differences in the NAO-driven AMOC response that are very

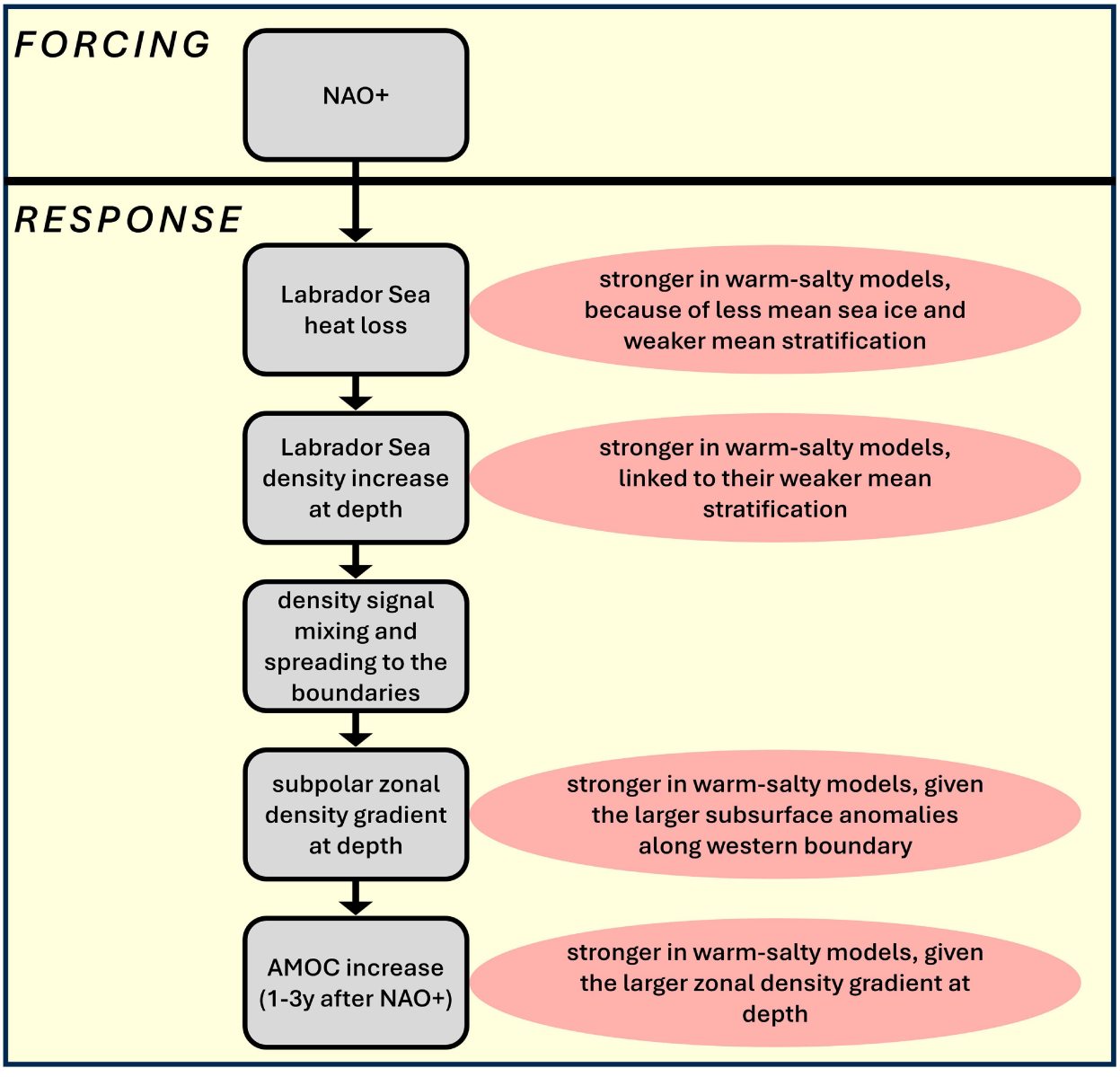

FIG. 10. Summarizing schematic of the proposed mechanism. The NAO forcing leading to a chain of responses is represented by the gray boxes. Mean state biases influencing these responses are shown to their right. The impacts are defined for the warm–salty models relative to the cold–fresh models.

similar to the original categorization (Fig. S3a). Furthermore, SPG density itself appears to also be related to the strength of NAO–AMOC relationships in models (e.g., Figs. 1 and 7), but still, it produces slightly weaker model differences (Fig. S3j).

The effect of nonstationarity in the models' mean states, e.g., regime shifts, and its effect on the categorization of each model were not investigated here. However, when testing the mean categorizations using standard errors (see Fig. 1), only one model (CNRM-ESM2-1) could potentially be classified in a different category (cold–salty rather than warm–salty in that case). Yet, this model remains included here, as a sensitivity test excluding it did not show different results. Further tests were also performed, like allowing different subsamples of models, e.g., all models in the warm–salty or cold–fresh category (not only those with NAO and AMOC data); or only models providing data for each variable listed in Table 1; or excluding the three E3SM models as they could be considered as outliers regarding their low SSS. None of these tests altered the main results. Sensitivity to the definition of AMOC, e.g., depth space rather than density coordinates, was not assessed. Future investigations could assess whether the results are impacted by the method of AMOC calculation, especially for AMOC at subpolar latitudes (cf. Fig. 6 from Hirschi et al. 2020).

b. What determines the category of a model?

A fundamental question arising here is as follows: What determines whether a model is warm–salty or cold–fresh? Although investigating this remains out of scope here, it is relevant for future work. The choice of parameterizations and physical constants are potential candidates to determine the SPG T and S properties, as models from the same centers tend to appear in clusters (Fig. 1). However, it is less clear whether there are similarities due to shared model components.

Model resolution is another potential candidate to determine a model's mean. In our sample of CMIP6 models, two model pairs differing only in resolution are included: HadGEM3-GC31-LL and HadGEM3-GC31-MM (nos. 25 and 26 in Table 1) and MPI-ESM1-2-LR and MPI-ESM1-2-HR (nos. 29 and 30 in Table 1). While the higher-resolution version of HadGEM3 is somewhat warmer and saltier than its lower-resolution version, there is almost no difference between the two MPI-ESM versions. It must be noted that it is not straightforward to compare the resolution of the model versions given the irregular structure of many grid types. For example, the two MPI-ESM versions have a similar resolution in the SPG area. Although we cannot find evidence that resolution is an important driver of differences here, Menary et al. (2015) and Jackson et al. (2020) concluded that higher resolution was related to warmer and saltier mean states. Furthermore, Hirschi et al. (2020) found that higher resolution was related to a stronger mean AMOC in a number of models (although many of them with the NEMO ocean component). Thus, the ultimate role of resolution should be addressed further. This is also motivated by the importance of representing small-scale processes, especially ocean eddies (Moreno-Chamarro et al. 2022; Roberts et al. 2016; Yeager et al. 2021).

c. Implications for uncertainty in future projections of the AMOC

Because of its role in climate, the projected future changes of the AMOC are of great interest. There is large uncertainty in the severity of the projected weakening, which is primarily due to the intermodel spread (Reintges et al. 2017). Some part of this spread is explained by the fact that models with a strong mean AMOC simulate a stronger decline under greenhouse gas forcing (Lin et al. 2023; Gregory et al. 2005; Rugenstein et al. 2013; Weijer et al. 2020; Winton et al. 2014). Specifically, Lin et al. (2023) demonstrated that CMIP6 models with a stronger mean AMOC also simulate a weaker LS stratification and a larger impact of the surface warming on subsurface densities which finally cause a stronger AMOC decline under greenhouse gas forcing. Taken together with our findings, these results underscore the necessity of improving the representation of the subpolar North Atlantic to enhance the accuracy of future AMOC predictions and projections.

d. Quality of model results

From comparison of both model categories with observations several characteristics (like Labrador Sea stratification and sea ice, mixed layer depth, and NAO-related heat fluxes), we have shown that warm–salty models appear more realistic compared to the cold–fresh models. However, the comparison with observational data can only provide an estimate of realism. For example, the model output analyzed here originates from preindustrial control experiments, whereas the observation-based datasets cover the years from 1960 onward. Yet, simulated changes in subpolar temperature and salinity over 1850–1960s (Zhu and Liu 2020) are small in comparison to the spread between models (Fig. 1). There might also be large errors in the observation-based datasets, especially in subsurface EN4 data, used to compute mixed layer depth. These errors, combined with the short period from 1960 onward, lead us to have limited trust in the detrended EN4 density regressions (Fig. S17). Nevertheless, some key anomalies seen in the warm–salty models agree with the EN4 data, especially the lag 1–3 years temperature-driven significant densification in the Labrador and Irminger Seas for 600- and 1000-m depths. We also note that the simulated AMOC response to the NAO could also be unrealistic if models are not correctly simulating all relevant processes. For example, models show a lack of density compensation in the Labrador Sea (Zou et al. 2020).

5. Summary and conclusions

In this study, we have analyzed CMIP6 preindustrial control data to understand how mean state differences in the North Atlantic subpolar gyre affect the strength of the NAO–AMOC relationship. The following key points were demonstrated:

1) There is large uncertainty in the CMIP6 models' mean states in surface SPG of the North Atlantic. If an individual model is warmer (colder) than the multimodel average, then it tends to be saltier (fresher) than the multimodel average. The spread is more than 6°C in SST and more than 4 psu in SSS.
2) Intermodel differences in the NAO-forced AMOC signal are sensitive to the metric of spiciness, i.e., the models' tendency to be warm–salty versus cold–fresh in the surface SPG. Warm–salty models are characterized by a significantly larger delayed AMOC response to the NAO compared to cold–fresh models, which is linked to buoyancy, not wind forcing. It should be noted that categorizing models based on other mean state biases than spiciness (e.g., the mean AMOC strength or the location of deep convection) could yield similar differences in the AMOC response to the NAO, which is due to the different biases in a model being physically linked.
3) Multiple lines of evidence suggest that warm–salty models are more realistic and that the NAO–AMOC relationship is too weak in cold–fresh models.

The explanation for the differences between the warm–salty and cold–fresh models can be summarized as follows (see also Fig. 10): in warm–salty models, the Labrador Sea has a much lower sea ice cover, leading to larger NAO-related heat loss. Additionally, the Labrador Sea has a weaker stratification and deeper convection in the warm–salty models. This enables the NAO buoyancy signal to reach greater depths in the warm–salty models compared to the cold–fresh models. Only in the warm–salty models is there a subsurface (1800-m depth) density increase propagating from the Labrador

Sea southward along the western boundary. These subsurface density anomalies create a zonal density gradient which can produce a stronger AMOC response to the NAO in those warm–salty models. We speculate that the subpolar surface spiciness is particularly relevant to discriminating the models' NAO–AMOC relationship because it combines effects from both the warm and saline surface conditions. For example, a warm surface state tends to enhance the NAO-driven surface buoyancy loss as it leads to reduced sea ice in the LS, enhancing the air–sea temperature contrast in winter. Furthermore, a more saline surface state enhances the LS surface density and, thus, reduces stratification. In this study, we have demonstrated that a combined metric that considers both effects is particularly effective for explaining the intermodel spread of the NAO–AMOC relationship. Several of our findings are supported by previous studies (e.g., Lin et al. 2023; Kim et al. 2023; Polo et al. 2014; Menary et al. 2015; Yeager et al. 2021; Jackson et al. 2020). Here, we present a mechanism explaining how the differences in mean state spiciness affect the AMOC response to the NAO by altering a chain of NAO-driven responses from heat flux to subsurface density signals.

It was demonstrated that large intermodel uncertainties and biases exist in the mean states and processes of the North Atlantic in CMIP6 models. This implies that results based on the output of a single model, or even a multimodel mean, should be interpreted carefully. Understanding the spread in results across multimodel comparisons will help to test their robustness. Such comparison can help to identify sources for uncertainty, providing a basis for model improvement.

Acknowledgments. A. R. was funded by the European Union's Marie Skłodowska-Curie Individual Fellowship DivPredSkill (101026271). J. R. and R. S. were funded by NERC via the WISHBONE (NE/T013516/1) and CANARI (NE/W004984/1) projects. Additionally, J. R. was funded by NERC via the SNAPDRAGON project (NE/T013494/1). S. Y. acknowledges support from the Regional and Global Model Analysis (RGMA) component of the Earth and Environmental System Modeling Program of the U.S. Department of Energy's Office of Biological and Environmental Research (BER) under Award DE-SC0022070. We acknowledge the World Climate Research Programme, which, through its Working Group on Coupled Modelling, coordinated and promoted CMIP6. We thank the climate modeling groups for producing and making available their model output, the Earth System Grid Federation (ESGF) for archiving the data and providing access, and the multiple funding agencies that support CMIP6 and ESGF. This work used JASMIN.

Data availability statement. The model CMIP6 data used here are open source and can be found through the different ESGF nodes (https://esgf.llnl.gov/nodes.html). The EN4 data are available at https://www.metoffice.gov.uk/hadobs/en4/index.html; HadSLP2 data are available at https://www.metoffice.gov.uk/hadobs/hadslp2/; the merged Hadley-OI SST and SIC data are available at https://gdex.ucar.edu/dataset/158_asphilli.html; and the ERA5 data are available at https://www.ecmwf.int/en/forecasts/dataset/ecmwf-reanalysis-v5. Analysis codes for reproducing the figures in this manuscript are available at https://doi.org/10.5281/zenodo.11200263.

REFERENCES

Allan, R., and T. Ansell, 2006: A new globally complete monthly historical gridded mean Sea Level Pressure dataset (HadSLP2): 1850–2004. *J. Climate*, **19**, 5816–5842, https://doi.org/10.1175/JCLI3937.1.

Ba, J., and Coauthors, 2014: A multi-model comparison of Atlantic multidecadal variability. *Climate Dyn.*, **43**, 2333–2348, https://doi.org/10.1007/s00382-014-2056-1.

Bellomo, K., M. Angeloni, S. Corti, and J. von Hardenberg, 2021: Future climate change shaped by inter-model differences in Atlantic meridional overturning circulation response. *Nat. Commun.*, **12**, 3659, https://doi.org/10.1038/s41467-021-24015-w.

Buckley, M. W., and J. Marshall, 2016: Observations, inferences, and mechanisms of the Atlantic meridional overturning circulation: A review. *Rev. Geophys.*, **54**, 5–63, https://doi.org/10.1002/2015RG000493.

Caesar, L., S. Rahmstorf, A. Robinson, G. Feulner, and V. Saba, 2018: Observed fingerprint of a weakening Atlantic Ocean overturning circulation. *Nature*, **556**, 191–196, https://doi.org/10.1038/s41586-018-0006-5.

——, G. D. McCarthy, D. J. R. Thornalley, N. Cahill, and S. Rahmstorf, 2021: Current Atlantic meridional overturning circulation weakest in last millennium. *Nat. Geosci.*, **14**, 118–120, https://doi.org/10.1038/s41561-021-00699-z.

Chafik, L., N. P. Holliday, S. Bacon, and T. Rossby, 2022: Irminger Sea is the center of action for subpolar AMOC variability. *Geophys. Res. Lett.*, **49**, e2022GL099133, https://doi.org/10.1029/2022GL099133.

Cheng, W., J. C. H. Chiang, and D. Zhang, 2013: Atlantic meridional overturning circulation (AMOC) in CMIP5 Models: RCP and historical simulations. *J. Climate*, **26**, 7187–7197, https://doi.org/10.1175/JCLI-D-12-00496.1.

Cunningham, S. A., and Coauthors, 2007: Temporal variability of the Atlantic meridional overturning circulation at 26.5°N. *Science*, **317**, 935–938, https://doi.org/10.1126/science.1141304.

Danabasoglu, G., 2008: On multidecadal variability of the Atlantic meridional overturning circulation in the community climate system model version 3. *J. Climate*, **21**, 5524–5544, https://doi.org/10.1175/2008JCLI2019.1.

Delworth, T. L., and F. Zeng, 2016: The impact of the North Atlantic Oscillation on climate through its influence on the Atlantic meridional overturning circulation. *J. Climate*, **29**, 941–962, https://doi.org/10.1175/JCLI-D-15-0396.1.

——, ——, L. Zhang, R. Zhang, G. A. Vecchia, and X. Yang, 2017: The central role of ocean dynamics in connecting the North Atlantic Oscillation to the extratropical component of the Atlantic multidecadal oscillation. *J. Climate*, **30**, 3789–3805, https://doi.org/10.1175/JCLI-D-16-0358.1.

Eyring, V., S. Bony, G. A. Meehl, C. A. Senior, B. Stevens, R. J. Stouffer, and K. E. Taylor, 2016: Overview of the Coupled Model Intercomparison Project Phase 6 (CMIP6) experimental design and organization. *Geosci. Model Dev.*, **9**, 1937–1958, https://doi.org/10.5194/gmd-9-1937-2016.

Good, S. A., M. J. Martin, and N. A. Rayner, 2013: EN4: Quality controlled ocean temperature and salinity profiles and monthly objective analyses with uncertainty estimates. *J. Geophys. Res. Oceans*, **118**, 6704–6716, https://doi.org/10.1002/2013JC009067.

Gregory, J. M., and Coauthors, 2005: A model intercomparison of changes in the Atlantic thermohaline circulation in response to increasing atmospheric CO_2 concentration. *Geophys. Res. Lett.*, **32**, L12703, https://doi.org/10.1029/2005GL023209.

Hersbach, H., and Coauthors, 2020: The ERA5 global reanalysis. *Quart. J. Roy. Meteor. Soc.*, **146**, 1999–2049, https://doi.org/10.1002/qj.3803.

Heuzé, C., 2017: North Atlantic deep water formation and AMOC in CMIP5 models. *Ocean Sci.*, **13**, 609–622, https://doi.org/10.5194/os-13-609-2017.

Hirschi, J. J.-M., and Coauthors, 2020: The Atlantic meridional overturning circulation in high-resolution models. *J. Geophys. Res. Oceans*, **125**, e2019JC015522, https://doi.org/10.1029/2019JC015522.

Hurrell, J. W., Y. Kushnir, G. Ottersen, and M. Visbeck, 2003: An overview of the North Atlantic Oscillation. *The North Atlantic Oscillation: Climatic Significance and Environmental Impact*, *Geophys. Monogr.*, Vol. 134, Amer. Geophys. Union, 1–35, https://doi.org/10.1029/134GM01.

Jackson, L. C., and T. Petit, 2023: North Atlantic overturning and water mass transformation in CMIP6 models. *Climate Dyn.*, **60**, 2871–2891, https://doi.org/10.1007/s00382-022-06448-1.

——, K. A. Peterson, C. D. Roberts, and R. A. Wood, 2016: Recent slowing of Atlantic overturning circulation as a recovery from earlier strengthening. *Nat. Geosci.*, **9**, 518–522, https://doi.org/10.1038/ngeo2715.

——, and Coauthors, 2019: The mean state and variability of the North Atlantic circulation: A perspective from ocean reanalyses. *J. Geophys. Res. Oceans*, **124**, 9141–9170, https://doi.org/10.1029/2019JC015210.

——, and Coauthors, 2020: Impact of ocean resolution and mean state on the rate of AMOC weakening. *Climate Dyn.*, **55**, 1711–1732, https://doi.org/10.1007/s00382-020-05345-9.

Khatri, H., R. G. Williams, T. Woollings, and D. M. Smith, 2022: Fast and slow subpolar ocean responses to the North Atlantic Oscillation: Thermal and dynamical changes. *Geophys. Res. Lett.*, **49**, e2022GL101480, https://doi.org/10.1029/2022GL101480.

Kilbourne, K. H., and Coauthors, 2022: Atlantic circulation change still uncertain. *Nat. Geosci.*, **15**, 165–167, https://doi.org/10.1038/s41561-022-00896-4.

Kim, H.-J., S.-I. An, J.-H. Park, M.-K. Sung, D. Kim, Y. Choi, and J.-S. Kim, 2023: North Atlantic Oscillation impact on the Atlantic meridional overturning circulation shaped by the mean state. *npj Climate Atmos. Sci.*, **6**, 25, https://doi.org/10.1038/s41612-023-00354-x.

Kim, W. M., S. Yeager, and G. Danabasoglu, 2020: Atlantic multidecadal variability and associated climate impacts initiated by ocean thermohaline dynamics. *J. Climate*, **33**, 1317–1334, https://doi.org/10.1175/JCLI-D-19-0530.1.

——, ——, and ——, 2021: Revisiting the causal connection between the Great Salinity Anomaly of the 1970s and the shutdown of Labrador Sea deep convection. *J. Climate*, **34**, 675–696, https://doi.org/10.1175/JCLI-D-20-0327.1.

——, Y. Ruprich-Robert, A. Zhao, S. Yeager, and J. Robson, 2024: North Atlantic response to observed North Atlantic Oscillation surface heat flux in three climate models. *J. Climate*, **37**, 1777–1796, https://doi.org/10.1175/JCLI-D-23-0301.1.

Kostov, Y., and Coauthors, 2021: Distinct sources of interannual subtropical and subpolar Atlantic overturning variability. *Nat. Geosci.*, **14**, 491–495, https://doi.org/10.1038/s41561-021-00759-4.

Kwon, Y.-O., and C. Frankignoul, 2012: Stochastically-driven multidecadal variability of the Atlantic meridional overturning circulation in CCSM3. *Climate Dyn.*, **38**, 859–876, https://doi.org/10.1007/s00382-011-1040-2.

Lai, W. K. M., J. I. Robson, L. J. Wilcox, and N. Dunstone, 2022: Mechanisms of internal Atlantic multidecadal variability in HadGEM3-GC3.1 at two different resolutions. *J. Climate*, **35**, 1365–1383, https://doi.org/10.1175/JCLI-D-21-0281.1.

Latif, M., J. Sun, M. Visbeck, and M. Hadi Bordbar, 2022: Natural variability has dominated Atlantic meridional overturning circulation since 1900. *Nat. Climate Change*, **12**, 455–460, https://doi.org/10.1038/s41558-022-01342-4.

Leith, C. E., 1973: The standard error of time-average estimates of climatic means. *J. Appl. Meteor.*, **12**, 1066–1069, https://doi.org/10.1175/1520-0450(1973)012<1066:TSEOTA>2.0.CO;2.

Lin, Y.-J., B. E. J. Rose, and Y.-T. Hwang, 2023: Mean state AMOC affects AMOC weakening through subsurface warming in the Labrador Sea. *J. Climate*, **36**, 3895–3915, https://doi.org/10.1175/JCLI-D-22-0464.1.

Liu, C., and Coauthors, 2022: Discrepancies in simulated ocean net surface heat fluxes over the North Atlantic. *Adv. Atmos. Sci.*, **39**, 1941–1955, https://doi.org/10.1007/s00376-022-1360-7.

Lohmann, K., H. Drange, and M. Bentsen, 2009: Response of the North Atlantic subpolar gyre to persistent North Atlantic Oscillation like forcing. *Climate Dyn.*, **32**, 273–285, https://doi.org/10.1007/s00382-008-0467-6.

Lozier, M. S., and Coauthors, 2017: Overturning in the subpolar North Atlantic program: A new international ocean observing system. *Bull. Amer. Meteor. Soc.*, **98**, 737–752, https://doi.org/10.1175/BAMS-D-16-0057.1.

Lumpkin, R., and K. Speer, 2007: Global ocean meridional overturning. *J. Phys. Oceanogr.*, **37**, 2550–2562, https://doi.org/10.1175/JPO3130.1.

Mecking, J. V., S. S. Drijfhout, L. C. Jackson, and T. Graham, 2016: Stable AMOC off state in an eddy-permitting coupled climate model. *Climate Dyn.*, **47**, 2455–2470, https://doi.org/10.1007/s00382-016-2975-0.

——, ——, ——, and M. B. Andrews, 2017: The effect of model bias on Atlantic freshwater transport and implications for AMOC bi-stability. *Tellus*, **69A**, 1299910, https://doi.org/10.1080/16000870.2017.1299910.

Megann, A., A. Blaker, S. Josey, A. New, and B. Sinha, 2021: Mechanisms for late 20th and early 21st century decadal AMOC variability. *J. Geophys. Res. Oceans*, **126**, e2021JC017865, https://doi.org/10.1029/2021JC017865.

Menary, M. B., D. L. R. Hodson, J. I. Robson, R. T. Sutton, R. A. Wood, and J. A. Hunt, 2015: Exploring the impact of CMIP5 model biases on the simulation of North Atlantic decadal variability. *Geophys. Res. Lett.*, **42**, 5926–5934, https://doi.org/10.1002/2015GL064360.

Moreno-Chamarro, E., and Coauthors, 2022: Impact of increased resolution on long-standing biases in HighResMIP-PRIMAVERA climate models. *Geosci. Model Dev.*, **15**, 269–289, https://doi.org/10.5194/gmd-15-269-2022.

Msadek, R., and Coauthors, 2014: Predicting a decadal shift in North Atlantic climate variability using the GFDL forecast system. *J. Climate*, **27**, 6472–6496, https://doi.org/10.1175/JCLI-D-13-00476.1.

Ortega, P., M. Montoya, F. González-Rouco, J. Mignot, and S. Legutke, 2012: Variability of the Atlantic meridional overturning circulation in the last millennium and two IPCC scenarios. *Climate Dyn.*, **38**, 1925–1947, https://doi.org/10.1007/s00382-011-1081-6.

——, J. Robson, R. T. Sutton, and M. B. Andrews, 2017: Mechanisms of decadal variability in the Labrador Sea and the wider North Atlantic in a high-resolution climate model. *Climate Dyn.*, **49**, 2625–2647, https://doi.org/10.1007/s00382-016-3467-y.

——, and Coauthors, 2021: Labrador Sea subsurface density as a precursor of multidecadal variability in the North Atlantic: A multi-model study. *Earth Syst. Dyn.*, **12**, 419–438, https://doi.org/10.5194/esd-12-419-2021.

Polo, I., J. Robson, R. Sutton, and M. A. Balmaseda, 2014: The importance of wind and buoyancy forcing for the boundary density variations and the geostrophic component of the AMOC at 26°N. *J. Phys. Oceanogr.*, **44**, 2387–2408, https://doi.org/10.1175/JPO-D-13-0264.1.

Reintges, A., T. Martin, M. Latif, and N. S. Keenlyside, 2017: Uncertainty in twenty-first century projections of the Atlantic meridional overturning circulation in CMIP3 and CMIP5 models. *Climate Dyn.*, **49**, 1495–1511, https://doi.org/10.1007/s00382-016-3180-x.

Rhines, P., S. Häkkinen, and S. A. Josey, 2008: Is oceanic heat transport significant in the climate system? *Arctic–Subarctic Ocean Fluxes*, Springer, 87–109.

Roach, L. A., E. Blanchard-Wrigglesworth, S. Ragen, W. Cheng, K. C. Armour, and C. M. Bitz, 2022: The impact of winds on AMOC in a fully-coupled climate model. *Geophys. Res. Lett.*, **49**, e2022GL101203, https://doi.org/10.1029/2022GL101203.

Roberts, M. J., H. T. Hewitt, P. Hyder, D. Ferreira, S. A. Josey, M. Mizielinski, and A. Shelly, 2016: Impact of ocean resolution on coupled air-sea fluxes and large-scale climate. *Geophys. Res. Lett.*, **43**, 10 430–10 438, https://doi.org/10.1002/2016GL070559.

Robson, J., R. Sutton, K. Lohmann, D. Smith, and M. D. Palmer, 2012: Causes of the rapid warming of the North Atlantic Ocean in the mid-1990s. *J. Climate*, **25**, 4116–4134, https://doi.org/10.1175/JCLI-D-11-00443.1.

——, I. Polo, D. L. R. Hodson, D. P. Stevens, and L. C. Shaffrey, 2018: Decadal prediction of the North Atlantic subpolar gyre in the HiGEM high-resolution climate model. *Climate Dyn.*, **50**, 921–937, https://doi.org/10.1007/s00382-017-3649-2.

——, and Coauthors, 2022: The role of anthropogenic aerosol forcing in the 1850–1985 strengthening of the AMOC in CMIP6 historical simulations. *J. Climate*, **35**, 6843–6863, https://doi.org/10.1175/JCLI-D-22-0124.1.

Robson, J. I., R. T. Sutton, and D. M. Smith, 2012: Initialized decadal predictions of the rapid warming of the North Atlantic Ocean in the mid 1990s. *Geophys. Res. Lett.*, **39**, L19713, https://doi.org/10.1029/2012GL053370.

Roussenov, V. M., R. G. Williams, M. S. Lozier, N. P. Holliday, and D. M. Smith, 2022: Historical reconstruction of subpolar North Atlantic overturning and its relationship to density. *J. Geophys. Res. Oceans*, **127**, e2021JC017732, https://doi.org/10.1029/2021JC017732.

Rugenstein, M. A. A., M. Winton, R. J. Stouffer, S. M. Griffies, and R. Hallberg, 2013: Northern high-latitude heat budget decomposition and transient warming. *J. Climate*, **26**, 609–621, https://doi.org/10.1175/JCLI-D-11-00695.1.

Scaife, A. A., C. K. Folland, L. V. Alexander, A. Moberg, and J. R. Knight, 2008: European climate extremes and the North Atlantic Oscillation. *J. Climate*, **21**, 72–83, https://doi.org/10.1175/2007JCLI1631.1.

——, and Coauthors, 2014: Skillful long-range prediction of European and North American winters. *Geophys. Res. Lett.*, **41**, 2514–2519, https://doi.org/10.1002/2014GL059637.

Schurer, A. P., G. C. Hegerl, H. Goosse, M. A. Bollasina, M. H. England, D. M. Smith, and S. F. B. Tett, 2023: Role of multidecadal variability of the winter North Atlantic oscillation on Northern Hemisphere climate. *Environ. Res. Lett.*, **18**, 044046, https://doi.org/10.1088/1748-9326/acc477.

Shea, D., J. Hurrell, and A. Phillips, 2022: Merged Hadley-OI sea surface temperature and sea ice concentration data set, version 6.0. UCAR/NCAR–GDEX, https://gdex.ucar.edu/dataset/158_asphilli/version/6.0.html.

Smith, D. M., and Coauthors, 2020: North Atlantic climate far more predictable than models imply. *Nature*, **583**, 796–800, https://doi.org/10.1038/s41586-020-2525-0.

Stramma, L., D. Kieke, M. Rhein, F. Schott, I. Yashayaev, and K. P. Koltermann, 2004: Deep water changes at the western boundary of the subpolar North Atlantic during 1996 to 2001. *Deep-Sea Res. I*, **51**, 1033–1056, https://doi.org/10.1016/j.dsr.2004.04.001.

Sutton, R. T., and B. Dong, 2012: Atlantic Ocean influence on a shift in European climate in the 1990s. *Nat. Geosci.*, **5**, 788–792, https://doi.org/10.1038/ngeo1595.

Treguier, A. M., and Coauthors, 2023: The mixed-layer depth in the Ocean Model Intercomparison Project (OMIP): Impact of resolving mesoscale eddies. *Geosci. Model Dev.*, **16**, 3849–3872, https://doi.org/10.5194/gmd-16-3849-2023.

Trenberth, K. E., Y. Zhang, J. T. Fasullo, and L. Cheng, 2019: Observation-based estimates of global and basin ocean meridional heat transport time series. *J. Climate*, **32**, 4567–4583, https://doi.org/10.1175/JCLI-D-18-0872.1.

Visbeck, M., E. P. Chassignet, R. G. Curry, T. L. Delworth, R. R. Dickson, and G. Krahmann, 2003: The ocean's response to North Atlantic Oscillation variability. *The North Atlantic Oscillation: Climatic Significance and Environmental Impact*, *Geophys. Monogr.*, Vol. 134, Amer. Geophys. Union, 113–145, https://doi.org/10.1029/134GM06.

Wang, C., L. Zhang, S.-K. Lee, L. Wu, and C. R. Mechoso, 2014: A global perspective on CMIP5 climate model biases. *Nat. Climate Change*, **4**, 201–205, https://doi.org/10.1038/nclimate2118.

Weaver, A. J., and Coauthors, 2012: Stability of the Atlantic meridional overturning circulation: A model intercomparison. *Geophys. Res. Lett.*, **39**, L20709, https://doi.org/10.1029/2012GL053763.

Wei, X., and R. Zhang, 2022: A simple conceptual model for the self-sustained multidecadal AMOC variability. *Geophys. Res. Lett.*, **49**, e2022GL099800, https://doi.org/10.1029/2022GL099800.

Weijer, W., W. Cheng, O. A. Garuba, A. Hu, and B. T. Nadiga, 2020: CMIP6 models predict significant 21st century decline of the Atlantic meridional overturning circulation. *Geophys. Res. Lett.*, **47**, e2019GL086075, https://doi.org/10.1029/2019GL086075.

Winton, M., W. G. Anderson, T. L. Delworth, S. M. Griffies, W. J. Hurlin, and A. Rosati, 2014: Has coarse ocean resolution biased simulations of transient climate sensitivity? *Geophys. Res. Lett.*, **41**, 8522–8529, https://doi.org/10.1002/2014GL061523.

Xu, X., E. P. Chassignet, and F. Wang, 2019: On the variability of the Atlantic meridional overturning circulation transports in coupled CMIP5 simulations. *Climate Dyn.*, **52**, 6511–6531, https://doi.org/10.1007/s00382-018-4529-0.

Yashayaev, I., 2007: Hydrographic changes in the Labrador Sea, 1960–2005. *Prog. Oceanogr.*, **73**, 242–276, https://doi.org/10.1016/j.pocean.2007.04.015.

Yeager, S., and G. Danabasoglu, 2014: The origins of late-twentieth-century variations in the large-scale North Atlantic circulation. *J. Climate*, **27**, 3222–3247, https://doi.org/10.1175/JCLI-D-13-00125.1.

——, A. Karspeck, G. Danabasoglu, J. Tribbia, and H. Teng, 2012: A decadal prediction case study: Late twentieth-century North Atlantic Ocean heat content. *J. Climate*, **25**, 5173–5189, https://doi.org/10.1175/JCLI-D-11-00595.1.

——, and Coauthors, 2021: An outsized role for the Labrador Sea in the multidecadal variability of the Atlantic overturning circulation. *Sci. Adv.*, **7**, eabh3592, https://doi.org/10.1126/sciadv.abh3592.

Yeager, S. G., and J. I. Robson, 2017: Recent progress in understanding and predicting Atlantic decadal climate variability. *Curr. Climate Change Rep.*, **3**, 112–127, https://doi.org/10.1007/s40641-017-0064-z.

Zhang, J., and R. Zhang, 2015: On the evolution of Atlantic meridional overturning circulation fingerprint and implications for decadal predictability in the North Atlantic. *Geophys. Res. Lett.*, **42**, 5419–5426, https://doi.org/10.1002/2015GL064596.

Zhang, R., 2017: On the persistence and coherence of subpolar sea surface temperature and salinity anomalies associated with the Atlantic multidecadal variability. *Geophys. Res. Lett.*, **44**, 7865–7875, https://doi.org/10.1002/2017GL074342.

——, R. Sutton, G. Danabasoglu, Y.-O. Kwon, R. Marsh, S. G. Yeager, D. E. Amrhein, and C. M. Little, 2019: A review of the role of the Atlantic meridional overturning circulation in Atlantic multidecadal variability and associated climate impacts. *Rev. Geophys.*, **57**, 316–375, https://doi.org/10.1029/2019RG000644.

Zhu, C., and Z. Liu, 2020: Weakening Atlantic overturning circulation causes South Atlantic salinity pile-up. *Nat. Climate Change*, **10**, 998–1003, https://doi.org/10.1038/s41558-020-0897-7.

Zou, S., M. S. Lozier, F. Li, R. Abernathey, and L. Jackson, 2020: Density-compensated overturning in the Labrador Sea. *Nat. Geosci.*, **13**, 121–126, https://doi.org/10.1038/s41561-019-0517-1.